

# Infinite-layer nickelates as Ni- $e_g$ Hund's metals

Byungkyun Kang,<sup>1</sup> Corey Melnick,<sup>1</sup> Patrick Semon,<sup>1</sup> Gabriel Kotliar,<sup>2,1</sup> and Sangkook Choi<sup>1,\*</sup>

<sup>1</sup>*Condensed Matter Physics and Materials Science Department,  
Brookhaven National Laboratory, Upton, NY 11973, USA*

<sup>2</sup>*Department of Physics and Astronomy, Rutgers University, New Jersey 08854, USA*  
(Dated: July 30, 2020)

The recent and exciting discovery of superconductivity in the hole-doped infinite-layer nickelate  $\text{Nd}_{1-\delta}\text{Sr}_\delta\text{NiO}_2$  draws strong attention to correlated quantum materials. From a theoretical view point, this new class of unconventional superconducting materials provide an opportunity to unveil new physics in correlated quantum materials. Here we study the temperature and doping dependence of the local spectrum of the charge, spin and orbital susceptibilities *from first principles*. By using *ab initio* LQSGW+DMFT methodology, we show that onsite Hund's coupling in Ni- $d$  orbitals gives rise to multiple signatures of Hund's metallic phase in Ni- $e_g$  orbitals. The proposed picture of the nickelates as an  $e_g$  (two orbit) Hund's metal differs from the picture of the Fe-based superconductors as a five orbital Hund's metal as well as the picture of the cuprates as doped charge transfer insulators. Our finding unveils a new class of the Hund's metals and has potential implications for the broad range of correlated two orbital systems away from half-filling.

*Introduction.* Although the mechanisms of unconventional superconductivity remain elusive, the discoveries of new classes of unconventional superconductors have proliferated experimentally. These experimental efforts revived the interest in correlated quantum materials and provided opportunities to unveil new physics hidden within them. To illustrate, in the cuprate superconductors [1], superconductivity emerges by doping a charge transfer insulator [2], where the on-site Hubbard interaction ( $U$ ) localizes electrons such that their quasiparticle weight vanishes [3, 4]. According to the theory of conventional superconductors, it is improbable that this bad-metallic phase would support superconductivity. This motivated the theoretical proposals of superconducting pairing mechanisms beyond the Bardeen-Cooper-Schrieffer (BCS) paradigm [5–7]. This in turn lead to the discovery of other unconventional superconductors wherein a superconducting phase emerged from the bad-metal "parent" state, and this bad-metal state did not necessarily form due to a strong the Hubbard interaction. For example, in the multi-orbital Fe-based superconductors [8, 9], the on-site Hund's coupling ( $J$ ) promotes bad metallic behavior in their normal phase [10–13]. This gives rise to the new concept of the Hund's metal [14, 15], which plays the role of a reliable reference system for Fe-based superconducting materials [12, 14–20] and ruthenates [12, 21–24].

Recently, the thrilling discovery of Ni-based superconductors [25–28] turns the spotlight on correlated quantum materials and their unconventional superconductivity [29, 30].  $\text{Nd}_{0.8}\text{Sr}_{0.2}\text{NiO}_2$  and infinite-layer cuprates, e.g.  $\text{CaCuO}_2$ , are isostructural [31, 32], where the two dimensional Ni-O plane is geometrically analogous to the Cu-O plane in the cuprate. The Ni- $d_{x^2-y^2}$  orbital of each  $\text{Ni}^{1+}$  ion can be expected to be half-filled with an effective spin-1/2 on each site according to the oxidation state rules. In combination, this makes  $\text{Nd}_{0.8}\text{Sr}_{0.2}\text{NiO}_2$

a promising cuprate analog [33–38].

However, the differences from cuprates are striking. Its parent compound is seldom regarded as a charge transfer insulator [34, 39–41] and there is no sign of long-range magnetic orders [32] down to 1.7 K. In addition, its parent compound shows a resistivity upturn upon cooling [25], which is common in heavy-fermion superconductors and is often due to Kondo effects [42, 43]. The sign change of the Hall coefficient implies that electrons as well as holes may play an important role in the materials properties [25], implying its multi-orbital nature [43–45]. Moreover, it is debatable whether the doped hole forms a spin singlet or triplet doublon with the original hole on a Ni ion [46–52], suggesting possible Hund metal physics [43, 53, 54]. These similarities and differences to various unconventional superconductors are puzzling, but they do provide a chance to explore hidden aspects of electron correlation.

In this paper, we will investigate a new aspect of the multi-orbital physics in infinite-layer nickelates *from first principles*. By using *ab initio* LQSGW+DMFT methodology [55, 56], a parameter-free electronic structure method targeting correlated quantum materials, we calculate the electronic structure of infinite layer nickelates. In particular, we will investigate the role of Hund's coupling in the temperature and doping dependence of the local spectrum of the charge, spin and orbital susceptibilities. We found multiple signatures of "Hundness" associated with the Ni- $d$  subshell in both the parent and doped compounds. In particular, we found that Hundness becomes apparent among the Ni- $e_g$  orbitals but not the Ni- $t_{2g}$  orbitals, wherein the Hundness is strongly suppressed by the inactivity of the Ni- $t_{2g}$  orbitals.

*Methods.* Following the literature [33, 42, 52, 53, 57–60], we studied  $\text{La}_{1-\delta}\text{Ba}_\delta\text{NiO}_2$  instead of  $\text{Nd}_{1-\delta}\text{Sr}_\delta\text{NiO}_2$  to avoid the difficulty in the treatment of the Nd- $4f$  band. This is acceptable, as it has been reported

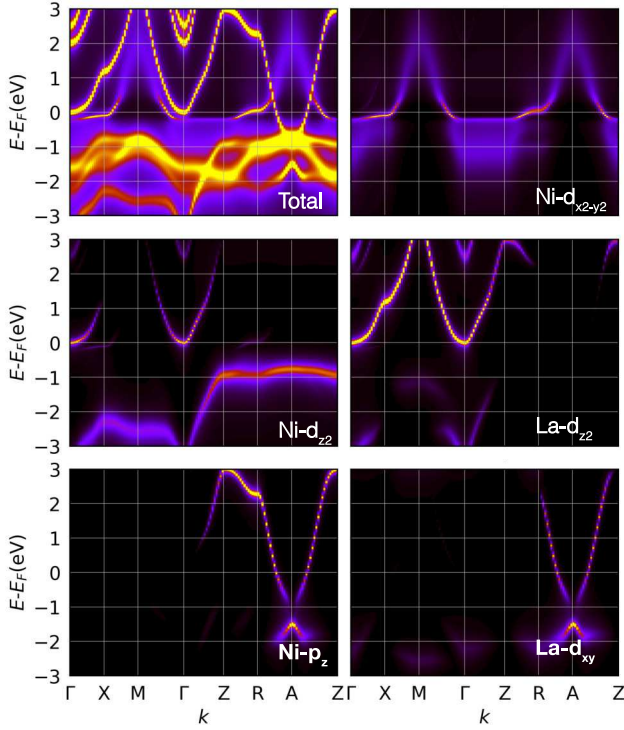


FIG. 1. Total and orbital-resolved spectral function of  $\text{La}_{0.8}\text{Ba}_{0.2}\text{NiO}_2$  along a high-symmetry line as calculated within *ab initio* LQSGW+DMFT at  $T=300\text{K}$ . Of the two bands crossing the Fermi level, the lower energy band shows  $\text{Ni-d}_{x^2-y^2}$  character, and the other, self-doping band at higher energy is a mixture of  $\text{La-d}_{z^2}$ ,  $\text{Ni-d}_{z^2}$ ,  $\text{La-d}_{xy}$  and  $\text{Ni-p}_z$ .

that  $\text{La}_{1-\delta}\text{Ba}_\delta\text{NiO}_2$  has a similar electronic structure to  $\text{Nd}_{1-\delta}\text{Sr}_\delta\text{NiO}_2$ . Here we note that there are reports that intra-atomic  $4f$ - $5d$  exchange coupling in Nd atom can induce spin-disorder broadening of the electron pockets [61] and the Nd  $f$  orbital can hybridize strongly with the  $\text{Ni-d}_{x^2-y^2}$  orbital [62]. The effect of Ba doping has been treated within the virtual crystal approximation. For the LQSGW+DMFT scheme, the code ComDMFT [56] was used. For the LQSGW part of the LQSGW+DMFT scheme, the code FlapwMBPT [63] was used. For the details of electronic structure calculation, please see the supplementary materials.

**Results and Discussions.** The low-energy electronic structure of  $\text{La}_{1-\delta}\text{Ba}_\delta\text{NiO}_2$  shows multi-orbital characters. In particular, the two bands crossing the Fermi energy have substantial  $\text{Ni-e}_g$  orbital character. Fig. 1 shows the electronic structure of  $\text{La}_{0.8}\text{Ba}_{0.2}\text{NiO}_2$  within *ab initio* LQSGW+DMFT. Consistent with the results obtained with other electronic structure methodologies such as DFT [33, 36, 37, 42–44, 52, 60, 62, 64–68], DFT+DMFT [34, 53], one-shot  $G_0W_0$  [59], the total spectral function shows that there are two bands crossing the Fermi level. Of these two bands, the lower energy band shows strong two dimensional character, and it is dominated by the  $\text{Ni-d}_{x^2-y^2}$  orbitals. The remaining

TABLE I. Electron occupation of  $\text{Ni-d}$  orbitals in  $\text{La}_{0.8}\text{Ba}_{0.2}\text{NiO}_2$  and  $\text{Fe-d}$  orbitals in  $\text{FeSe}$  at  $T=300\text{K}$

Materials	$d_{xy}$	$d_{yz}$	$d_{xz}$	$d_{z^2}$	$d_{x^2-y^2}$
$\text{La}_{0.8}\text{Ba}_{0.2}\text{NiO}_2$	1.94	1.90	1.90	1.60	1.0
$\text{FeSe}$	1.22	1.19	1.19	1.44	1.26

band, the so called self-doping band, is a higher energy band which shows strong hybridization between other Ni orbitals and La orbitals. The band dispersion varies strongly along the direction normal to the Ni-O plane ( $\hat{z}$ ), demonstrating the strong 3-dimensional character of the self-doping band [42]. Moreover, the orbital character of the self-doping band is strongly dependent on  $k_z$ . In the  $k_z=0$  plane, the orbital character of the self-doping band is mostly  $\text{La-d}_{z^2}$  and  $\text{Ni-d}_{z^2}$  [64, 65]. In contrast, in the  $k_z = \pi/c$  plane, where  $c$  is the lattice constant along the  $\hat{z}$  direction, its orbital character is mostly  $\text{La-d}_{xy}$  and  $\text{Ni-p}_z$ . This analysis is consistent with recent two band model study from *first-principles*, showing that the two Fermi-level-crossing bands can be spanned by a  $\text{Ni-d}_{x^2-y^2}$  orbital and an axial orbital [44]. The axial orbital is not centered on a single atom. Instead, its density is centered on both the Ni and La atoms.

Orbital occupation in the  $\text{Ni-d}$  orbitals differentiates the  $t_{2g}$  and  $e_g$  orbitals. As summarized in Table I, the  $\text{Ni-e}_g$  orbitals are partially filled but the  $\text{Ni-t}_{2g}$  orbitals are fully filled in  $\text{La}_{0.8}\text{Ba}_{0.2}\text{NiO}_2$ . This orbital occupation profile is far from a prediction based on oxidation state rules, *i.e.*, 2, 2, 2, 2, and 1 for  $\text{Ni-d}_{xy}$ ,  $\text{Ni-d}_{yz}$ ,  $\text{Ni-d}_{xz}$ ,  $\text{Ni-d}_{z^2}$ , and  $\text{Ni-d}_{x^2-y^2}$ , respectively. Intriguingly, the difference stands out especially for the  $\text{Ni-z}^2$  orbital, which is far from the expected double occupation [54, 57]. This discrepancy can be explained by the hybridization between  $\text{Ni-d}_{z^2}$  and  $\text{La-d}_{z^2}$  orbitals. The strong hybridization between these two orbitals in the  $\Gamma$ -X-M- $\Gamma$  plane makes the  $\text{Ni-d}_{z^2}$  orbital exhibit a dispersion which is distinct from its dispersion in isolation (the flat band at  $E_F-1\text{eV}$  in the  $Z$ -R-A-Z plane in Fig. 1(c)) [69]. Indeed, upon Ba doping up to 0.3, only  $\sim 25\%$  of the added holes go into the  $\text{Ni-d}$  orbitals, while the remaining holes go into other orbitals, especially the  $\text{La-d}_{xy}$ ,  $\text{La-d}_z$  and  $\text{Ni-p}_z$  orbitals (as shown in the supplementary materials). This is consistent with other theoretical studies at low-doping [34, 64], and it makes the  $t_{2g}$ - $e_g$  differentiation in orbital occupation robust against extrinsic hole-doping. Here we note that the orbital occupation as well as the orbital resolved spectral functions are dependent on the choice of the Wannier orbitals. To construct atomic-orbital-like Wannier orbitals tightly bounded and centered on the atoms, we constructed 31 atom-centered Wannier orbitals for each spin (see the supplementary materials).

To reveal the signatures of Hundness and Mottness, we calculate the temperature and doping dependence of

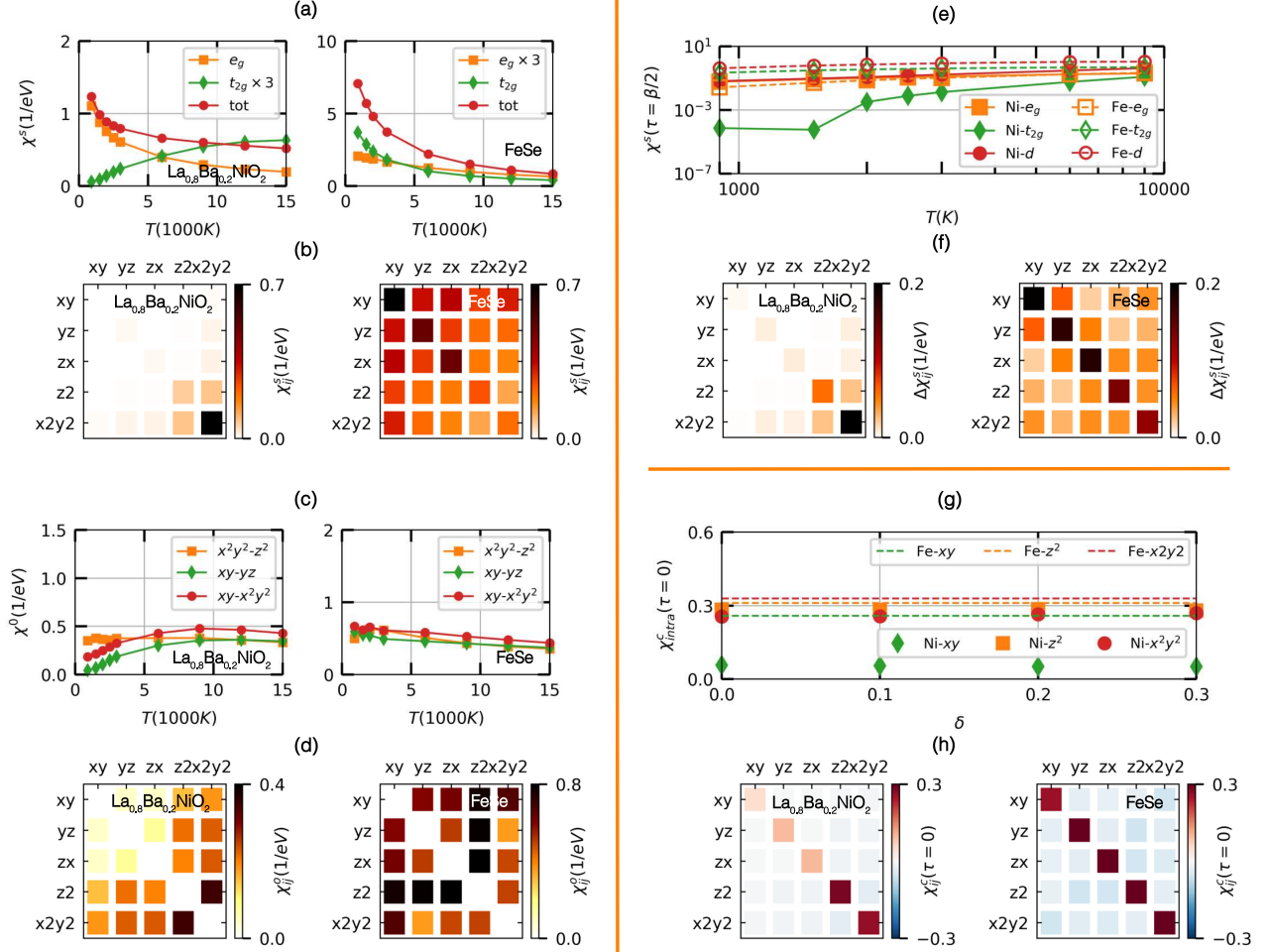


FIG. 2. The temperature and doping dependence of the local spectrum of the charge, spin and orbital susceptibilities. (a) The temperature dependence of static spin susceptibility ( $\chi^s$ ) of  $d$  orbitals (red dots),  $t_{2g}$  orbitals (green diamonds), and  $e_g$ -orbitals (orange squares) in  $\text{La}_{0.8}\text{Ba}_{0.2}\text{NiO}_2$  and FeSe. (b) Orbital-resolved static spin susceptibility ( $\chi^s_{ij}$ ) of Ni- $d$  orbitals in  $\text{La}_{0.8}\text{Ba}_{0.2}\text{NiO}_2$  and Fe- $d$  orbitals in FeSe at  $T = 900$  K. (c) The temperature dependence of static orbital susceptibility ( $\chi^o_{ij}$ ) of Ni- $d$  orbitals in  $\text{La}_{0.8}\text{Ba}_{0.2}\text{NiO}_2$  and Fe- $d$  orbitals in FeSe. (d) Orbital susceptibility ( $\chi^o_{ij}$ ) of Ni- $d$  orbitals in  $\text{La}_{0.8}\text{Ba}_{0.2}\text{NiO}_2$  and Fe- $d$  orbitals in FeSe at  $T = 900$  K. (e) The temperature dependence of  $\chi^s(\tau = \beta/2)$  of  $d$  orbitals (red dots),  $t_{2g}$  orbitals (green diamonds), and  $e_g$ -orbitals (orange squares) in  $\text{La}_{0.8}\text{Ba}_{0.2}\text{NiO}_2$  (filled markers) and FeSe (empty markers). (f) Orbital-resolved dynamical contribution of spin susceptibility ( $\Delta\chi^s_{ij}$ ) of Ni- $d$  orbitals in  $\text{La}_{0.8}\text{Ba}_{0.2}\text{NiO}_2$  and Fe- $d$  orbitals in FeSe at  $T=900$  K. (g) The doping dependence of instantaneous intraorbital charge susceptibility ( $\chi^c_{ii}(\tau = 0)$ ) of  $d$  orbitals in  $\text{La}_{0.8}\text{Ba}_{0.2}\text{NiO}_2$  (markers) and FeSe (dashed lines). (e) Instantaneous charge susceptibility ( $\chi^c_{ij}(\tau = 0)$ ) of Ni- $d$  orbitals in  $\text{La}_{0.8}\text{Ba}_{0.2}\text{NiO}_2$  and Fe- $d$  orbitals in FeSe at  $T = 900$  K.

the local spectrum of the charge, spin and orbital susceptibilities and check if there are signatures of Hundness: spin-orbital separation, enhanced dynamical spin susceptibility, and orbital decoupling. Although five Ni- $d$  orbitals in  $\text{La}_{1-\delta}\text{Ba}_\delta\text{NiO}_2$  show several key signatures of a Hund's metal, these signatures are primarily evident in the active Ni- $e_g$  orbitals and not the inactive Ni- $t_{2g}$  orbitals.

Five Ni- $d$  orbitals in  $\text{La}_{1-\delta}\text{Ba}_\delta\text{NiO}_2$  show clear spin-orbital separation. Fig. 2(a) and Fig. 2(c) show the temperature dependence of the static local susceptibility in spin ( $\chi^s_{tot}$ ) and orbital ( $\chi^o_{ij}$ ) chan-

nels. These are defined as  $\chi^s_{tot} = \int_0^\beta d\tau \chi^s_{tot}(\tau)$ , and  $\chi^o_{ij} = \int_0^\beta d\tau \chi^o_{ij}(\tau)$ . Here  $\chi^s_{tot}(\tau) = \sum_{i,j=\text{Ni-d}} \chi^s_{ij}(\tau)$ ,  $\chi^s_{ij}(\tau) = \sum_{\sigma,\sigma'=\uparrow,\downarrow} (-1)^{1+\delta_{\sigma\sigma'}} \chi_{i\sigma;j\sigma'}(\tau)/4$ ,  $\chi^o_{ij}(\tau) = \sum_{k,l=i,j} \sum_{\sigma,\sigma'=\uparrow,\downarrow} (-1)^{1+\delta_{kl}} \chi_{k\sigma;l\sigma'}(\tau)$ ,  $\chi_{i\sigma;j\sigma'}(\tau) = \langle \Delta n_{i\sigma}(\tau) \Delta n_{j\sigma'}(0) \rangle$ , and  $\Delta n_{i\sigma}(\tau) = n_{i\sigma}(\tau) - \langle n_{i\sigma}(\tau) \rangle$ . According to Deng *et al.* [70], the temperatures at which the screening of the spin and orbital degrees of freedom becomes noticeable are one of the key measures with which to distinguish between Mott and Hund physics. These onset screening temperatures in spin and orbital channels can be obtained by estimating the temperature at which these susceptibilities deviates from Curie-like

behaviors. In the Mott regime, these two energy scales coincide. In contrast, in the Hund regime, the orbital onset temperature is much higher than the spin onset temperature. At a temperature between these two onset temperatures, the spin susceptibility is Curie-like but the orbital-susceptibility is Pauli-like. This is exactly the behavior seen in FeSe. In FeSe, the local spin susceptibility is Curie-like (red dots in Fig. 2(a)), but the local orbital susceptibility approaches its maximum upon cooling (red dots in Fig. 2(c)).  $\text{La}_{0.8}\text{Ba}_{0.2}\text{NiO}_2$  behaves like FeSe. The spin degree of freedom (red dots in Fig. 2(a)) shows Curie-like behavior. In contrast, the orbital susceptibility between any Ni- $d$  orbital pair shows a downturn of the susceptibility upon cooling (red dots in Fig. 2(c)).

Five Ni- $d$  orbitals in  $\text{La}_{1-\delta}\text{Ba}_\delta\text{NiO}_2$  show enhanced dynamical spin susceptibility. According to Werner et al. [21], at the spin-freezing crossover regime where Hundness dominates the electron correlation, the system shows enhanced  $\chi_{\text{tot}}^s(\tau = \beta/2)$  [57] and it increases linearly upon heating. The coefficient of linear term can be related to NMR relaxation rates [71]. If Hundness gets stronger, the system shows sublinear temperature dependence. As shown in Fig 2(e), both Fe- $d$  (empty red dots) orbitals in FeSe and Ni- $d$  orbitals (filled red dots) in  $\text{La}_{1-\delta}\text{Ba}_\delta\text{NiO}_2$  show sublinear dependence in temperature.

Five Ni- $d$  orbitals in  $\text{La}_{1-\delta}\text{Ba}_\delta\text{NiO}_2$  show orbital decoupling behavior, much like the Fe- $d$  orbitals in FeSe. According to de' Medici [11], a Hund's metal shows orbital decoupling and this manifests in the suppressed instantaneous interorbital charge susceptibility ( $\chi_{i \neq j}^c(\tau = 0)$ ) while the intraorbital susceptibility ( $\chi_{i=j}^c(\tau = 0)$ ) is finite [13, 72]. Here,  $\chi_{ij}^c(\tau = 0) = \sum_{\sigma, \sigma' = \uparrow, \downarrow} \chi_{i\sigma; j\sigma'}(\tau = 0)$ . Fe- $d$  orbitals in FeSe show the predicted orbital decoupling, as shown in Fig. 2 (h).  $\chi_{i \neq j}^c(\tau = 0)$  between any two pairs of Fe- $d$  orbitals is negative and strongly suppressed in comparison to any intraorbital one. Similarly, the interorbital, instantaneous charge susceptibility is suppressed in the Ni- $d$  orbitals of  $\text{La}_{1-\delta}\text{Ba}_\delta\text{NiO}_2$ .

However, there is an important distinction between the Ni- $d$  orbitals in  $\text{La}_{1-\delta}\text{Ba}_\delta\text{NiO}_2$  and Fe- $d$  orbitals in FeSe: The  $t_{2g}$  orbitals in  $\text{La}_{1-\delta}\text{Ba}_\delta\text{NiO}_2$  are inactive. This is anticipated from the electron occupation of Ni- $t_{2g}$  orbitals listed in Table I. The idea of inactive  $t_{2g}$  orbitals in  $\text{La}_{1-\delta}\text{Ba}_\delta\text{NiO}_2$  can be demonstrated further by examining the local susceptibilities in the spin, orbital, and charge channels. This makes it difficult to conclude that  $\text{La}_{1-\delta}\text{Ba}_\delta\text{NiO}_2$  is a canonical  $d$ -orbital Hund's metal. Let us discuss.

First, spin fluctuations are active only in the Ni- $e_g$  orbitals, as shown in Fig. 2 (b), which depicts  $\chi_{ij}^s = \int_0^\beta d\tau \chi_{ij}^s(\tau)$ . In FeSe, all possible pairs of Fe- $d$  orbitals show a strong spin response. In contrast, only the Ni- $e_g$  subspace exhibits a strong spin response in  $\text{La}_{0.8}\text{Ba}_{0.2}\text{NiO}_2$ , while the response due to the remaining

pairs is strongly suppressed. The temperature dependence of the spin susceptibility in the  $t_{2g}$  subspace ( $\chi_{t_{2g}}^s$ ) further supports the distinction between the Ni- $d$  orbital and Fe- $d$  orbitals. Here,  $\chi_{t_{2g}}^s = \sum_{ij=t_{2g}} \int_0^\beta d\tau \chi_{ij}^s(\tau)$ . As shown in Fig. 2 (a),  $\chi_{t_{2g}}^s$  (green diamonds) in  $\text{La}_{0.8}\text{Ba}_{0.2}\text{NiO}_2$  strongly deviates from the Curie-like behaviors of  $\chi_{\text{tot}}^s$ . This does not occur in FeSe. Most strikingly,  $\chi_{t_{2g}}^s$  approaches zero upon cooling.

The temperature dependence of  $\chi^s(\tau = \beta/2)$  also support that the  $t_{2g}$  orbitals are inactive, as shown in Fig. 2 (e), which depicts  $\chi_{t_{2g}}^s(\tau = \beta/2) = \sum_{ij=t_{2g}} \chi_{ij}^s(\tau = \beta/2)$ . In contrast to the Fe- $d$  orbitals in FeSe where  $\chi_{t_{2g}}^s(\tau = \beta/2)$  (empty green diamonds) shows sublinear temperature dependence similar to  $\chi_{\text{tot}}^s(\tau = \beta/2)$ ,  $\chi_{t_{2g}}^s(\tau = \beta/2)$  of the Ni- $d$  orbitals in  $\text{La}_{0.8}\text{Ba}_{0.2}\text{NiO}_2$  (filled green diamonds) is essentially zero over a wide range of temperatures.

The dynamical contribution to the local spin susceptibility ( $\Delta\chi_{ij}^s$ ) provides additional evidence that the Ni- $t_{2g}$  orbitals are inactive. Here  $\Delta\chi_{ij}^s = \int_0^\beta d\tau \{\chi_{ij}^s(\tau) - \chi_{ij}^s(\tau = \beta/2)\}$ . According to Werner et al. [21], in the spin-freezing crossover regime where Hundness dominates, the system has a large spin susceptibility ( $\chi^s$ ) with a suppressed  $\Delta\chi^s$ . As shown in Fig. 2 (f), all possible pairs of  $\Delta\chi_{i,j}^s$  in FeSe are active. In contrast, the Ni- $e_g$  orbital contributions dominate in  $\text{La}_{0.8}\text{Ba}_{0.2}\text{NiO}_2$ .

Second, the static orbital susceptibility shows the suppression of orbital fluctuations in the Ni- $t_{2g}$  subspace, as shown in Fig. 2 (d), which depicts  $\chi_{ij}^o$ . In FeSe, all possible pairs of Fe- $d$  orbitals show a strong orbital response. In contrast, the  $\chi_{ij}^o$  in the Ni- $t_{2g}$  subspace are strongly suppressed in  $\text{La}_{0.8}\text{Ba}_{0.2}\text{NiO}_2$ . The temperature dependence of the orbital susceptibility in the  $t_{2g}$  subspace ( $\chi_{xy,yz}^o$ ), shown in Fig. 2 (c), is another distinction between Ni- $d$  orbitals and Fe- $d$  orbitals. Here, In contrast to FeSe, where  $\chi_{xy,yz}^o$  (green diamonds) follows  $\chi_{x^2-y^2,z^2}^o$  (orange squares),  $\chi_{xy,yz}^o$  (green diamonds) in  $\text{La}_{0.8}\text{Ba}_{0.2}\text{NiO}_2$  strongly deviates from  $\chi_{x^2-y^2,z^2}^o$  (orange squares). Most strikingly,  $\chi_{xy,yz}^o$  approaches zero upon cooling.

Third, the instantaneous charge susceptibility exhibits intraorbital charge fluctuations primarily in the Ni- $e_g$  subspace. Fig. 2 (g) and (h) show  $\chi_{ii}^c(\tau = 0)$ . In FeSe, all five intraorbital components are similar in magnitude. In contrast,  $\chi_{ii=Ni-t_{2g}}^c(\tau = 0)$  is strongly suppressed in comparison to  $\chi_{ii=Ni-e_g}^c(\tau = 0)$  in  $\text{La}_{0.8}\text{Ba}_{0.2}\text{NiO}_2$ .

Once we narrow down our view from all Ni- $d$  orbitals into only the Ni- $e_g$  orbitals, we can successfully find all signatures of a Hund's metal in the temperature and doping dependence of the local spectrum of the charge, spin and orbital susceptibilities. Two Ni- $e_g$  orbitals in  $\text{La}_{1-\delta}\text{Ba}_\delta\text{NiO}_2$  show clear spin-orbital separation, as shown in Fig. 2(a) and Fig. 2(c), which depict the temperature dependence of static local spin ( $\chi_{e_g}^s$ ) and orbital ( $\chi_{x^2-y^2,z^2}^o$ ) susceptibility. Here  $\chi_{e_g}^s =$

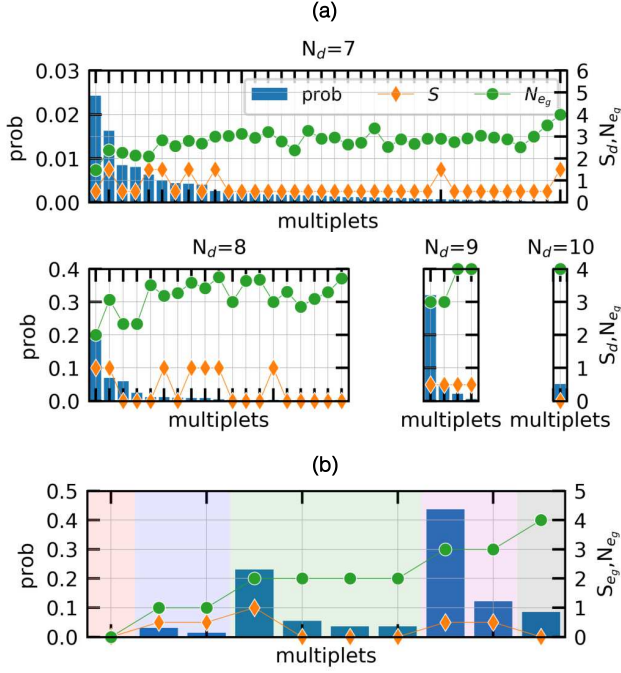


FIG. 3. (a) Reduced local many-body density on the Ni-3d multiplets in  $\text{La}_{0.8}\text{Ba}_{0.2}\text{NiO}_2$  at  $T=300\text{K}$ . Each multiplet has been labeled by using the Ni-3d total spin ( $S_d$ ) and Ni-3d total charge ( $N_d$ ). The Ni- $e_g$  total charge ( $N_{e_g}$ ) are also shown. (e) Reduced local many-body density on Ni- $e_g$  multiplets in  $\text{La}_{0.8}\text{Ba}_{0.2}\text{NiO}_2$  at  $T=300\text{K}$ . Each multiplet has been labeled by using Ni- $e_g$  total spin ( $S_{e_g}$ ) and Ni- $e_g$  total charge ( $N_{e_g}$ ).

$\sum_{ij=e_g} \int_0^\beta d\tau \chi_{ij}^s(\tau)$ . As in the case of  $\chi_{tot}^s$  (red circles),  $\chi_{e_g}^s$  (orange squares in Fig. 2(a)) shows Curie-like temperature dependence but  $\chi_{x^2-y^2, z^2}^o$  (orange squares in Fig. 2(c)) shows Pauli-like temperature dependence. Furthermore, Ni- $e_g$  orbitals in  $\text{La}_{1-\delta}\text{Ba}_\delta\text{NiO}_2$  show enhanced dynamical spin susceptibility. Fig. 2(e) shows  $\chi_{e_g}^s(\tau = \beta/2) = \sum_{ij=e_g} \chi_{ij}^s(\tau = \beta/2)$ . It shows that  $\chi_{e_g}^s(\tau = \beta/2)$  in Ni atom (filled orange squares) has a sublinear temperature dependence similar to  $\chi_{tot}^s(\tau = \beta/2)$ . Ni- $e_g$  orbitals in  $\text{La}_{1-\delta}\text{Ba}_\delta\text{NiO}_2$  show orbital decoupling behavior as the Fe- $d$  orbitals in FeSe. As shown in Fig. 2(h),  $\chi_{x^2-y^2, z^2}^o(\tau = 0)$  is strongly suppressed. Thus we conclude that  $\text{La}_{1-\delta}\text{Ba}_\delta\text{NiO}_2$  is a  $e_g$  Hund's metal: That is, the Hundness exists only among the Ni- $e_g$  orbitals.

To further clarify the microscopic origin of Ni- $e_g$  Hund's metallic behaviors, we investigate the reduced local many-body density or local probabilities of Ni-3d multiplet states in the atomic limit. Fig. 3 (a) shows the valence histogram for the Ni-3d multiplets in  $\text{La}_{0.8}\text{Ba}_{0.2}\text{NiO}_2$ . That is, it shows a partial trace over the density matrix of the full Hilbert space, where this partial trace excludes the Ni-3d subsystem in order to reveal the probability that a given multiplet state in the

correlated Ni-3d subsystem is occupied. We decompose the Ni-3d subspace according to the total charge ( $N_d$ ) of the multiplet states, and find that for  $N_d = 7, 8, 9$  and  $10$ , the most probable states involve the total spin  $S_d = 1/2, 1, 1/2$ , and  $0$  as well as the occupation of the  $e_g$  orbitals is  $1.47, 2, 3$ , and  $4$ , respectively. Interestingly, these can be interpreted as the multiplets which maximize the total spin of the Ni- $e_g$  electron in each  $N_{e_g}$  subspace; these are not the multiplets which maximize the total spin of all Ni-3d electrons in each  $N_d$  subspace. The reduced local many-body density on the Ni- $e_g$  multiplets shown in Fig. 3 (b) supports this observation. The most probable Ni- $e_g$  multiplet in each  $N_{e_g}$  subspace is the one with maximum Ni- $e_g$  total spin ( $S_{e_g}$ ). Again, this supports our conclusion that Hund metallic behaviors are limited to the Ni- $e_g$  orbitals.

*Conclusion.* By using *ab initio* LQSGW+DMFT methodology, we demonstrated that on-site Hund's coupling in Ni- $d$  orbitals results in multiple signatures of Hund's metallic phase in Ni- $e_g$  orbitals. Our finding sheds a new light on Hundness in the correlated quantum materials and has potential implications for the broad range of correlated two orbital systems and the role of on-site Hund's coupling away from half-filling [11, 49, 73].

*Acknowledgments.* S.C. thanks S. Ryee and C.-J. Kang for useful conversation. This work was supported by the U.S. Department of Energy, Office of Science, Basic Energy Sciences as a part of the Computational Materials Science Program. This research used resources of the National Energy Research Scientific Computing Center (NERSC), a U.S. Department of Energy Office of Science User Facility operated under Contract No. DE-AC02-05CH11231.

\* E-mail me at: sachoi@bnl.gov

- [1] J. G. Bednorz and K. A. Müller, Z. Physik B - Condensed Matter **64**, 189 (1986).
- [2] J. Zaanen, G. A. Sawatzky, and J. W. Allen, Phys. Rev. Lett. **55**, 418 (1985).
- [3] N. F. Mott and R. Peierls, Proc. Phys. Soc. **49**, 72 (1937).
- [4] N. F. Mott, Proc. Phys. Soc. A **62**, 416 (1949).
- [5] P. A. Lee, N. Nagaosa, and X.-G. Wen, Rev. Mod. Phys. **78**, 17 (2006), publisher: American Physical Society.
- [6] A. Garg, M. Randeria, and N. Trivedi, Nature Physics **4**, 762 (2008), number: 10 Publisher: Nature Publishing Group.
- [7] B. Keimer, S. A. Kivelson, M. R. Norman, S. Uchida, and J. Zaanen, Nature **518**, 179 (2015), number: 7538 Publisher: Nature Publishing Group.
- [8] Y. Kamihara, H. Hiramatsu, M. Hirano, R. Kawamura, H. Yanagi, T. Kamiya, and H. Hosono, J. Am. Chem. Soc. **128**, 10012 (2006), publisher: American Chemical Society.
- [9] Y. Kamihara, T. Watanabe, M. Hirano, and H. Hosono,

- J. Am. Chem. Soc. **130**, 3296 (2008), publisher: American Chemical Society.
- [10] L. de Medici, J. Mravlje, and A. Georges, Phys. Rev. Lett. **107**, 256401 (2011).
- [11] L. de Medici, Phys. Rev. B **83**, 205112 (2011).
- [12] A. Georges, L. de Medici, and J. Mravlje, Annual Review of Condensed Matter Physics **4**, 137 (2013).
- [13] A. Isidori, M. Berovi, L. Fanfarillo, L. de Medici, M. Fabrizio, and M. Capone, Phys. Rev. Lett. **122**, 186401 (2019).
- [14] K. Haule and G. Kotliar, New J. Phys. **11**, 025021 (2009).
- [15] Z. P. Yin, K. Haule, and G. Kotliar, Nature Materials **10**, 932 (2011).
- [16] L. de Medici, Phys. Rev. Lett. **118**, 167003 (2017), tex.ids: demedici\_HundInducedFermiLiquid\_2017a, demedici\_SupplementaryHundInduced2017.
- [17] N. Lanat, H. U. R. Strand, G. Giovannetti, B. Hellsing, L. de' Medici, and M. Capone, Phys. Rev. B **87**, 045122 (2013), publisher: American Physical Society.
- [18] P. Villar Arribi and L. de Medici, Phys. Rev. Lett. **121**, 197001 (2018), publisher: American Physical Society.
- [19] E. Bascones, B. Valenzuela, and M. J. Calderin, Phys. Rev. B **86**, 174508 (2012), publisher: American Physical Society.
- [20] S. Ryee, P. Smon, M. J. Han, and S. Choi, npj Quantum Mater. **5**, 1 (2020), number: 1 Publisher: Nature Publishing Group.
- [21] P. Werner, E. Gull, M. Troyer, and A. J. Millis, Phys. Rev. Lett. **101**, 166405 (2008).
- [22] J. Mravlje, M. Aichhorn, T. Miyake, K. Haule, G. Kotliar, and A. Georges, Phys. Rev. Lett. **106**, 096401 (2011), publisher: American Physical Society.
- [23] S. Hoshino and P. Werner, Phys. Rev. Lett. **115**, 247001 (2015).
- [24] J. Mravlje and A. Georges, Phys. Rev. Lett. **117**, 036401 (2016), publisher: American Physical Society.
- [25] D. Li, K. Lee, B. Y. Wang, M. Osada, S. Crossley, H. R. Lee, Y. Cui, Y. Hikita, and H. Y. Hwang, Nature **572**, 624 (2019).
- [26] D. Li, B. Y. Wang, K. Lee, S. P. Harvey, M. Osada, B. H. Goodge, L. Kourkoutis, and H. Hwang, Phys. Rev. Lett. **125**, 027001 (2020), publisher: American Physical Society.
- [27] Q. Gu, Y. Li, S. Wan, H. Li, W. Guo, H. Yang, Q. Li, X. Zhu, X. Pan, Y. Nie, and H.-H. Wen, arXiv:2006.13123 [cond-mat] (2020), arXiv: 2006.13123.
- [28] S. Zeng, C. S. Tang, X. Yin, C. Li, Z. Huang, J. Hu, W. Liu, G. J. Omar, H. Jani, Z. S. Lim, K. Han, D. Wan, P. Yang, A. T. S. Wee, and A. Ariando, arXiv:2004.11281 [cond-mat] (2020), arXiv: 2004.11281.
- [29] G. A. Sawatzky, Nature **572**, 592 (2019).
- [30] Y. Xiang, Q. Li, Y. Li, H. Yang, Y. Nie, and H.-H. Wen, arXiv:2007.04884 [cond-mat] (2020), arXiv: 2007.04884.
- [31] M. A. Hayward, M. A. Green, M. J. Rosseinsky, and J. Sloan, J. Am. Chem. Soc. **121**, 8843 (1999), publisher: American Chemical Society.
- [32] M. A. Hayward and M. J. Rosseinsky, Solid State Sciences International Conference on Inorganic Materials.
- [33] A. Botana and M. Norman, Phys. Rev. X **10**, 011024 (2020), publisher: American Physical Society.
- [34] M. Kitatani, L. Si, O. Janson, R. Arita, Z. Zhong, and K. Held, arXiv:2002.12230 [cond-mat] (2020), arXiv: 2002.12230.
- [35] J. E. Hirsch and F. Marsiglio, Physica C: Superconductivity and its Applications **566**, 1353534 (2020).
- [36] X. Wu, D. Di Sante, T. Schwemmer, W. Hanke, H. Y. Hwang, S. Raghu, and R. Thomale, Phys. Rev. B **101**, 060504 (2020), publisher: American Physical Society.
- [37] J. Karp, A. S. Botana, M. R. Norman, H. Park, M. Zingl, and A. Millis, Phys. Rev. X **10**, 021061 (2020), publisher: American Physical Society.
- [38] Z.-J. Lang, R. Jiang, and W. Ku, arXiv:2005.00022 [cond-mat] (2020), arXiv: 2005.00022.
- [39] A. Ikeda, T. Manabe, and M. Naito, Physica C: Superconductivity **495**, 134 (2013).
- [40] A. Ikeda, Y. Krockenberger, H. Irie, M. Naito, and H. Yamamoto, Appl. Phys. Express **9**, 061101 (2016).
- [41] Y. Fu, L. Wang, H. Cheng, S. Pei, X. Zhou, J. Chen, S. Wang, R. Zhao, W. Jiang, C. Liu, M. Huang, X. Wang, Y. Zhao, D. Yu, S. Wang, and J.-W. Mei, arXiv:1911.03177 [cond-mat] (2019), arXiv: 1911.03177.
- [42] M. Hepting, D. Li, C. J. Jia, H. Lu, E. Paris, Y. Tseng, X. Feng, M. Osada, E. Been, Y. Hikita, Y.-D. Chuang, Z. Hussain, K. J. Zhou, A. Nag, M. Garcia-Fernandez, M. Rossi, H. Y. Huang, D. J. Huang, Z. X. Shen, T. Schmitt, H. Y. Hwang, B. Moritz, J. Zaanen, T. P. Devereaux, and W. S. Lee, Nature Materials **19**, 381 (2020), number: 4 Publisher: Nature Publishing Group.
- [43] F. Lechermann, arXiv:2005.01166 [cond-mat] (2020), arXiv: 2005.01166.
- [44] P. Adhikary, S. Bandyopadhyay, T. Das, I. Dasgupta, and T. Saha-Dasgupta, arXiv:2005.01243 [cond-mat, physics:quant-ph] (2020), arXiv: 2005.01243.
- [45] B. H. Goodge, D. Li, M. Osada, B. Y. Wang, K. Lee, G. A. Sawatzky, H. Y. Hwang, and L. F. Kourkoutis, arXiv:2005.02847 [cond-mat] (2020), arXiv: 2005.02847.
- [46] M. Jiang, M. Berciu, and G. A. Sawatzky, Phys. Rev. Lett. **124**, 207004 (2020), publisher: American Physical Society.
- [47] Y.-H. Zhang and A. Vishwanath, Phys. Rev. Research **2**, 023112 (2020), publisher: American Physical Society.
- [48] L.-H. Hu and C. Wu, Phys. Rev. Research **1**, 032046 (2019).
- [49] P. Werner and S. Hoshino, Phys. Rev. B **101**, 041104 (2020), publisher: American Physical Society.
- [50] G.-M. Zhang, Y.-f. Yang, and F.-C. Zhang, Phys. Rev. B **101**, 020501 (2020), publisher: American Physical Society.
- [51] J. Chang, J. Zhao, and Y. Ding, arXiv:1911.12731 [cond-mat] (2019), arXiv: 1911.12731.

- [52] H. Sakakibara, H. Usui, K. Suzuki, T. Kotani, H. Aoki, and K. Kuroki, arXiv:1909.00060 [cond-mat] (2019), arXiv: 1909.00060.
- [53] Y. Wang, C.-J. Kang, H. Miao, and G. Kotliar, arXiv:2006.15305 [cond-mat] (2020), arXiv: 2006.15305.
- [54] F. Petocchi, V. Christiansson, F. Nilsson, F. Aryasetiawan, and P. Werner, arXiv:2006.00394 [cond-mat] (2020), arXiv: 2006.00394.
- [55] S. Choi, A. Kutevov, K. Haule, M. van Schilfgaarde, and G. Kotliar, npj Quantum Materials **1**, 16001 (2016).
- [56] S. Choi, P. Semon, B. Kang, A. Kutevov, and G. Kotliar, Computer Physics Communications **244**, 277 (2019).
- [57] I. Leonov, S. L. Skornyakov, and S. Y. Savrasov, Phys. Rev. B **101**, 241108 (2020), publisher: American Physical Society.
- [58] S. Ryee, H. Yoon, T. J. Kim, M. Y. Jeong, and M. J. Han, Phys. Rev. B **101**, 064513 (2020), publisher: American Physical Society.
- [59] V. Olevano, F. Bernardini, X. Blase, and A. Cano, Phys. Rev. B **101**, 161102 (2020), arXiv: 2001.09194.
- [60] F. Bernardini, V. Olevano, and A. Cano, arXiv:1910.13269 [cond-mat] (2019), arXiv: 1910.13269.
- [61] M.-Y. Choi, K.-W. Lee, and W. E. Pickett, Phys. Rev. B **101**, 020503 (2020).
- [62] P. Jiang, L. Si, Z. Liao, and Z. Zhong, Phys. Rev. B **100**, 201106 (2019).
- [63] A. Kutevov, V. Oudovenko, and G. Kotliar, Computer Physics Communications **219**, 407 (2017).
- [64] F. Lechermann, Phys. Rev. B **101**, 081110 (2020), publisher: American Physical Society.
- [65] K.-W. Lee and W. E. Pickett, Phys. Rev. B **70**, 165109 (2004).
- [66] H. Zhang, L. Jin, S. Wang, B. Xi, X. Shi, F. Ye, and J.-W. Mei, (2019).
- [67] E. Been, W.-S. Lee, H. Y. Hwang, Y. Cui, J. Zaanen, T. Devereaux, B. Moritz, and C. Jia, arXiv:2002.12300 [cond-mat] (2020), arXiv: 2002.12300.
- [68] Y. Gu, S. Zhu, X. Wang, J. Hu, and H. Chen, Communications Physics **3**, 1 (2020), number: 1 Publisher: Nature Publishing Group.
- [69] M.-Y. Choi, W. E. Pickett, and K.-W. Lee, arXiv:2005.03234 [cond-mat] (2020), arXiv: 2005.03234.
- [70] X. Deng, K. M. Stadler, K. Haule, A. Weichselbaum, J. von Delft, and G. Kotliar, Nat Commun **10**, 2721 (2019).
- [71] M. Randeria, N. Trivedi, A. Moreo, and R. T. Scalettar, Phys. Rev. Lett. **69**, 2001 (1992), publisher: American Physical Society.
- [72] L. Fanfarillo, J. Mansart, P. Toulemonde, H. Cercellier, P. Le Fèvre, F. Bertran, B. Valenzuela, L. Benfatto, and V. Brouet, Physical Review B **94** (2016), 10.1103/PhysRevB.94.155138.
- [73] K. M. Stadler, *A model study of strong correlations in Hund metals*, Text.PhDThesis, Ludwig-Maximilians-Universitt Mnchen (2019).

# Supplementary materials for “Infinite-layer nickelates as Ni- $e_g$ Hund’s metals”

Byungkyun Kang,<sup>1</sup> Corey Melnick,<sup>1</sup> Patrick Semon,<sup>1</sup> Gabriel Kotliar,<sup>2,1</sup> and Sangkook Choi<sup>1</sup>

<sup>1</sup>*Condensed Matter Physics and Materials Science Department,  
Brookhaven National Laboratory, Upton, NY 11973, USA*

<sup>2</sup>*Department of Physics and Astronomy, Rutgers University, New Jersey 08854, USA*  
(Dated: July 30, 2020)

## LQSGW CALCULATION

LQSGW calculations are performed by using FlapwMBPT package [1], which is based on full-potential linearized augmented plane wave plus local orbital method. For  $\text{La}_{1-\delta}\text{Ba}_\delta\text{NiO}_2$ , experimental lattice constants and atomic positions [2] for  $\text{NdNiO}_2$  are used. The Muffin-tin (MT) radius ( $R$ ) is selected as follows: 2.7 for La/Ba, 2.1 for Ni, and 1.8 for O in Bohr radius. Wave functions are spanned by spherical harmonics with  $l$  up to 8 for La/Ba, 6 for Cu, and 6 for O in the MT spheres. In the interstitial region (IS), it is spanned by plane waves with the cutoff ( $K_{\text{cut}}$ ) of  $R_{\text{Ni}}K_{\text{cut}} = 8.8$ . Product basis set is spanned by spherical harmonics with  $l$  up to 8 for La/Ba, 6 for Cu, and 6 for O in the MT spheres and by planewaves with the cutoff ( $G_{\text{cut}}$ ) of  $R_{\text{Ni}}G_{\text{cut}} = 13$  in IS region. All the unoccupied states are taken into account for both polarizability and self-energy calculation. The Brillouin zone is sampled in 444 grid.

For FeSe and NiO, please see this paper[3].

## WANNIER FUNCTION CONSTRUCTIONS

For  $\text{La}_{1-\delta}\text{Ba}_\delta\text{NiO}_2$ , 31 Wannier functions are constructed with a frozen energy window between -10 eV to 11.2 eV and with disentanglement energy window of -10 eV to 52 eV: La-s, La-p, La-d, La-f, Ni-s, Ni-p, Ni-d, and O-p orbitals. Initial trial orbitals are constructed by using Muffin-tin orbitals in LAPW basis set with well-defined angular momentum characters. Final Wannier orbitals are centered exactly at the targeted atom. Their orbital characters, calculated Wannier centers, and spreads are in Table I. Here, atomic positions of La, Ni and two O are (1.960000, 1.960000, 1.640000), (0.000000, 0.000000, 0.000000), (0.000000, 1.960000, 0.000000) and (1.960000, 0.000000, 0.000000), respectively.

## CONSTRAINED RANDOM PHASE APPROXIMATION

We calculated the bosonic Weiss field  $\tilde{U}$  associated with the correlated  $d$  orbitals within constrained random phase approximation (cRPA) [4, 5] and its Slater’s integrals. Here we stress that the bosonic Weiss field  $\tilde{U}$  from cRPA is a way to evaluate  $\tilde{U}$  and not identical to  $\tilde{U}$  from ideal fully self-consistent GW+EDMFT. Within cRPA, the bosonic Weiss field  $\tilde{U}$  is obtained by separating out the RPA polarizability ( $P_{QP}^{\text{low}}$ ) from the correlated states. In ComDMFT  $P_{QP}^{\text{low}}$  is defined by identifying correlated bands [5–7]. These are bands having strong Ni- $d$  orbital characters are chosen as correlated bands at each  $\mathbf{k}$  point. The number of correlated bands is set to be the number of correlated orbitals for each spin.

Then,  $P_{QP}^{\text{low}}$  is defined in the following way.

$$P_{QP}^{\text{low}}(\mathbf{r}, \mathbf{r}', \mathbf{k}, i\nu_n) = -2 \sum_{\mathbf{k}'} \sum_{\substack{\text{unoccupied} \\ \text{correlated bands}}}^N \sum_{\substack{\text{occupied} \\ \text{correlated bands}}}^M \psi_{N\mathbf{k}'}(\mathbf{r}) \psi_{M\mathbf{k}'+\mathbf{k}}^*(\mathbf{r}) \psi_{N\mathbf{k}'}^*(\mathbf{r}') \psi_{M\mathbf{k}'+\mathbf{k}}(\mathbf{r}') \frac{2(E_{N\mathbf{k}'} - E_{M\mathbf{k}'+\mathbf{k}})}{\nu_n^2 - (E_{N\mathbf{k}'} - E_{M\mathbf{k}'+\mathbf{k}})^2}, \quad (1)$$

Here,  $\psi_{N\mathbf{k}}(\mathbf{r})$  and  $E_{n\mathbf{k}}$  are quasiparticle wave function and quasiparticle energy with a band index  $N$  and crystal momentum vector  $\mathbf{k}$ , respectively.

TABLE I. Wannier function orbital characters, calculated wannier centers, and spreads of  $\text{La}_{0.8}\text{Ba}_{0.2}\text{NiO}_2$ 

orbital	type	center	spread ( $\text{\AA}^2$ )
1	La- $s$	( 1.960000, 1.960000, 1.640000 )	2.74772016
2	La- $p_y$	( 1.960000, 1.960000, 1.640000 )	2.62769922
3	La- $p_z$	( 1.960000, 1.960000, 1.640000 )	2.44701728
4	La- $p_x$	( 1.960000, 1.960000, 1.640000 )	2.62769922
5	La- $d_{xy}$	( 1.960000, 1.960000, 1.640000 )	2.14236838
6	La- $d_{yz}$	( 1.960000, 1.960000, 1.640000 )	1.89698543
7	La- $d_{z^2}$	( 1.960000, 1.960000, 1.640000 )	2.01022884
8	La- $d_{xz}$	( 1.960000, 1.960000, 1.640000 )	1.89698543
9	La- $d_{x^2-y^2}$	( 1.960000, 1.960000, 1.640000 )	1.95727422
10	La- $f_{y(3x^2-y^2)}$	( 1.960000, 1.960000, 1.640000 )	1.08079931
11	La- $f_{xyz}$	( 1.960000, 1.960000, 1.640000 )	1.16139012
12	La- $f_{yz^2}$	( 1.960000, 1.960000, 1.640000 )	1.00988505
13	La- $f_{z^3}$	( 1.960000, 1.960000, 1.640000 )	0.84709070
14	La- $f_{xz^2}$	( 1.960000, 1.960000, 1.640000 )	1.00988505
15	La- $f_{z(x^2-y^2)}$	( 1.960000, 1.960000, 1.640000 )	0.73111829
16	La- $f_{x(x^2-3y^2)}$	( 1.960000, 1.960000, 1.640000 )	1.08079931
17	Ni- $s$	( 0.000000, -0.000000, 0.000000 )	1.84519013
18	Ni- $p_y$	( -0.000000, 0.000000, -0.000000 )	1.57878888
19	Ni- $p_z$	( -0.000000, 0.000000, -0.000000 )	1.92206829
20	Ni- $p_x$	( 0.000000, -0.000000, -0.000000 )	1.57878888
21	Ni- $d_{xy}$	( 0.000000, -0.000000, -0.000000 )	0.39838710
22	Ni- $d_{yz}$	( -0.000000, -0.000000, -0.000000 )	0.38935269
23	Ni- $d_{z^2}$	( -0.000000, 0.000000, -0.000000 )	0.34985191
24	Ni- $d_{xz}$	( -0.000000, -0.000000, -0.000000 )	0.38935269
25	Ni- $d_{x^2-y^2}$	( -0.000000, 0.000000, 0.000000 )	0.31000163
26	O- $p_y$	( -0.000000, 1.960000, -0.000000 )	0.56811085
27	O- $p_z$	( -0.000000, 1.960000, -0.000000 )	0.78206995
28	O- $p_x$	( -0.000000, 1.960000, 0.000000 )	0.82293584
29	O- $p_y$	( 1.960000, -0.000000, -0.000000 )	0.82293584
30	O- $p_z$	( 1.960000, -0.000000, -0.000000 )	0.78206995
31	O- $p_x$	( 1.960000, -0.000000, -0.000000 )	0.56811085

Using  $P_{QP}^{high} = P_{QP} - P_{QP}^{low}$  where  $P_{QP}$  is RPA polarizability, the partially-screened Coulomb interaction ( $W_r$ ) is calculated by

$$W_r^{-1}(\mathbf{r}, \mathbf{r}', \mathbf{k}, i\nu_n) = V^{-1}(\mathbf{r}, \mathbf{r}', \mathbf{k}) - P_{QP}^{high}(\mathbf{r}, \mathbf{r}', \mathbf{k}, i\nu_n). \quad (2)$$

Next, Slater's integrals ( $F^k$ ) [8, 9] are calculated using  $W_r(\mathbf{r}, \mathbf{r}', \mathbf{R} = 0, i\nu_n)$  and Wannier functions for the correlated orbitals. Here we note that Slater parameterization of Coulomb interaction tensor is an approximation by assuming full rotation symmetry.

$$\begin{aligned}
F^k(i\nu_n) = & \frac{1}{C_k^l} \frac{4\pi}{2k+1} \sum_{m_1, m_2, m_3, m_4} \sum_{m'_1, m'_2, m'_3, m'_4} \\
& \langle Y_l^{m_1} | Y_k^{m_1-m_4} Y_l^{m_4} \rangle \langle Y_l^{m_2} Y_k^{m_2-m_3} | Y_l^{m_3} \rangle \\
& S_{m_1 m'_1} S_{m_2 m'_2} S_{m_3 m'_3}^{-1} S_{m_4 m'_4}^{-1} \int d\mathbf{r} d\mathbf{r}' W_r(\mathbf{r}, \mathbf{r}', R=0, i\nu_n) \\
& W_{R=0, m'_1}^*(\mathbf{r}) W_{R=0, m'_2}^*(\mathbf{r}') W_{R=0, m'_3}(\mathbf{r}') W_{R=0, m'_4}(\mathbf{r}),
\end{aligned} \quad (3)$$

where  $C_k^l = \frac{(2l+1)^4}{2k+1} \begin{bmatrix} l & k & l \\ 0 & 0 & 0 \end{bmatrix}$ ,  $\begin{bmatrix} l & k & l \\ 0 & 0 & 0 \end{bmatrix}$  is the Racah-Wigner 3j-symbol,  $S_{m_1 m'_1} = \langle Y_{lm_1} | Y_l^m \rangle$ ,  $|Y_l^m\rangle$  is spherical harmonics, and  $|Y_{lm}\rangle$  is cubic spherical harmonics.  $W_{\mathbf{R}, m}(\mathbf{r})$  is a Wannier function for a correlated orbital with angular part of cubic spherical harmonics  $Y_{lm}$  in the unicell at  $\mathbf{R}$ .

## DOUBLE COUNTING ENERGY

The electron self-energy included in both *ab initio* LQSGW and DMFT are the local Hartree term and the local GW term. They can be calculated as follows.

$$\tilde{\Sigma}_{DC,i,j}(i\omega_n) = 2 \sum_{k,l=m'_l} \tilde{G}_{l,k}(\tau=0^-) \tilde{U}_{iklj}(i\nu=0) - \sum_{k,l} \int d\tau \tilde{G}_{l,k}(\tau) \tilde{W}_{ikjl}(\tau) e^{i\omega_n \tau}. \quad (4)$$

where  $i,j,k$  and  $l$  are orbital indices.  $\tilde{G}$  is the local Green's function.  $\tilde{U}$  is constructed by using Slater's integrals in eq. (3).

$$\begin{aligned} \tilde{U}_{i,j,k,l}(i\nu_n) = & \sum_{m'_1 m'_2, m'_3 m'_4} S_{i,m_1} S_{j,m_2} S_{k,m_3}^{-1} S_{l,m_4}^{-1} \\ & \sum_{k=0}^{2l, \text{even}} \frac{4\pi}{2k+1} \langle Y_l^{m'_1} | Y_k^q Y_l^{m'_4} \rangle \langle Y_l^{m'_2} Y_k^q | Y_l^{m'_3} \rangle F^k(i\nu_n). \end{aligned} \quad (5)$$

Here, we assume that the frequency dependent interaction is of the form

$$\tilde{U}_{ijkl}(i\nu_n) = \tilde{U}_{ijkl} + F^0(i\nu_n) \delta_{il} \delta_{jk}, \quad (6)$$

that is, only the dynamical screening of the Slater-Condon parameter  $F^0$  is taken into account. The other Slater-Condon parameters, which define  $\tilde{U}_{ijkl}$ , are frequency independent and approximated by their value at  $\nu_n = \infty$ .  $\tilde{W}$  is the local screened Coulomb interaction given by

$$\tilde{W}_{ikjl}(i\nu_n) = \tilde{U}_{ikjl}(i\nu_n) + \sum_{mnpq} \tilde{U}_{imnl}(i\nu_n) \tilde{P}_{mpqn}(i\nu_n) \tilde{W}_{pkjq}(i\nu_n), \quad (7)$$

where  $\tilde{P}$  is the local polarizability and it is calculated as

$$\tilde{P}_{mpqn}(i\nu_n) = \int d\tau \tilde{G}_{n,p}(\tau) \tilde{G}_{q,m}(-\tau) e^{i\nu_n \tau}. \quad (8)$$

## DMFT SELF-CONSISTENT EQUATION

At each iteration of fermionic DMFT self-consistent loop, fermionic Weiss-field is constructed in the following way.

$$\tilde{G} = \left( \left( \frac{1}{N_{\mathbf{k}}} \sum_{\mathbf{k}} f_{\mathbf{k}}^\dagger G(\mathbf{k}, i\omega_n) f_{\mathbf{k}} \right)^{-1} + \tilde{\Sigma}_{imp} \right)^{-1} \quad (9)$$

Here  $f_{\mathbf{k}}$  is the fermionic projection operator to correlation orbitals (five Ni-d orbitals) and given by  $f_{\mathbf{k}} = \langle \mathbf{r} | W_{i\mathbf{k}} \rangle$  where  $|W_{i\mathbf{k}}\rangle = \frac{1}{\sqrt{N_{\mathbf{k}}}} \sum_{\mathbf{R}} |W_{i\mathbf{R}}\rangle e^{i\mathbf{k} \cdot \mathbf{R}}$ .  $\tilde{\Sigma}_{imp}$  is impurity self-energy from impurity solver. Within *ab initio* LQSGW+DMFT, lattice Green's function is calculated by embedding impurity self-energy into the LQSGW Green's function

$$G^{-1}(\mathbf{k}, i\omega_n) = i\omega_n - H_{QP}^{nl}(\mathbf{k}) - f_{\mathbf{k}} \tilde{\Sigma}_{imp}(i\omega_n) f_{\mathbf{k}}^\dagger, \quad (10)$$

where,  $H_{QP}^{nl}$  is non-local LQSGW hamiltonian[10], in which double-counting self-energy is compensated up to linear order in frequency.

$$H_{QP}^{nl}(\mathbf{k}) = \sqrt{Z_{DC}^{-1}(\mathbf{k})} H_{QP} \sqrt{Z_{DC}^{-1}(\mathbf{k})} - f_{\mathbf{k}} \tilde{\Sigma}_{DC}(\omega=0) f_{\mathbf{k}}^\dagger. \quad (11)$$

Here,  $H_{QP}$  is Wannier interpolated LQSGW Hamiltonian into  $15 \times 15 \times 15$   $k$ -grid.  $Z_{DC}^{-1}(\mathbf{k}) = 1 - f_{\mathbf{k}} \left( \partial \tilde{\Sigma}_{DC}(\omega=0) / \partial i\omega_n \right) f_{\mathbf{k}}^\dagger$ .

ComDMFT necessitates the solution of an impurity model action. In ComDMFT, hybridization-expansion continuous time quantum Monte Carlo (CTQMC) is adopted. CTQMC is a stochastic approach to obtain numerically exact

solutions of an impurity model. An impurity model consists of a small interacting system, the impurity, immersed in a bath of non-interacting electrons. The action of the impurity model relevant for GW+DMFT reads

$$S = - \int \int_0^\beta \sum_{ij} c_i^\dagger(\tau) \tilde{\mathcal{G}}_{ij}^{-1}(\tau - \tau') c_j(\tau') d\tau d\tau' + \frac{1}{2} \int \int_0^\beta \sum_{ijkl} c_i^\dagger(\tau) c_j^\dagger(\tau') \tilde{\mathcal{U}}_{ijkl}(\tau - \tau') c_k(\tau') c_l(\tau) d\tau d\tau', \quad (12)$$

where  $c_i^\dagger$  creates an electron in the generalized orbital  $i$  (which includes both spin and orbital degrees of freedom),  $\beta$  is the inverse temperature,  $\tilde{\mathcal{G}}_{ij}$  is the fermionic Weiss field in eq. (9) and  $\tilde{\mathcal{U}}_{ijkl}$  in eq. (5).

We assume that the frequency dependent interaction is of the form

$$\tilde{\mathcal{U}}_{ijkl}(i\nu_n) = \tilde{U}_{ijkl} + F^0(i\nu_n) \delta_{il} \delta_{jk}, \quad (13)$$

that is, only the dynamical screening of the Slater-Condon parameter  $F^0$  is taken into account, for the simplicity in the numerical algorithm based on hybridization-expansion CTQMC. The other Slater-Condon parameters, which define  $\tilde{U}_{ijkl}$ , are frequency independent and approximated by their value at  $\nu_n = \infty$ .

### ORBITAL-RESOLVED SPECTRAL FUCTION OF UNDOPED LANIO<sub>2</sub>

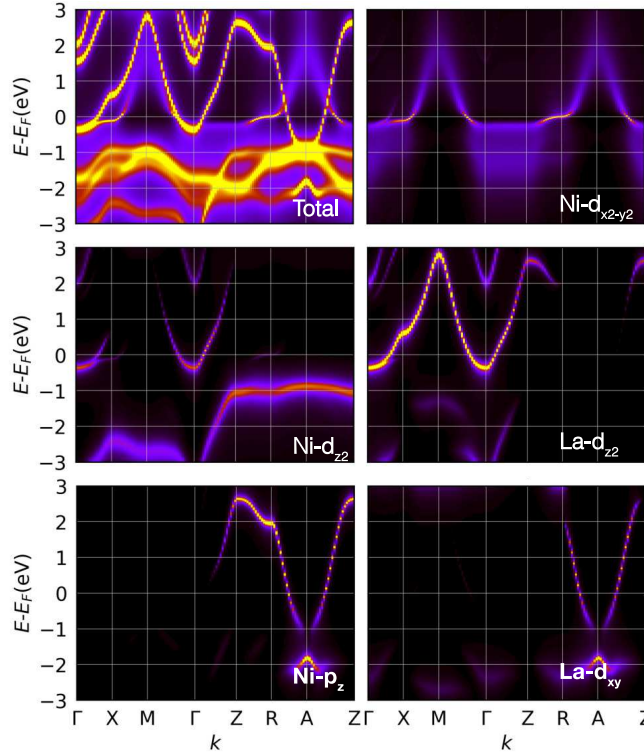


FIG. 1. Total and orbital-resolved spectral function of LaNiO<sub>2</sub> along a high-symmetry line within *ab initio* LQSGW+DMFT. Among the two bands crossing the Fermi level, the lower energy band shows Ni- $d_{x^2-y^2}$  character. The other self-doping band at higher energy is a mixture of four different orbitals. In the  $\Gamma$ -X-M- $\Gamma$  plane, its orbital characters are La- $d_{z^2}$  and Ni- $d_{z^2}$ . In the Z-R-A-Z plane, its orbital characters are La- $d_{xy}$  and Ni- $p_z$ .

Fig. 1 shows total and orbital-resolved spectral function of LaNiO<sub>2</sub> along a high-symmetry line within *ab initio* LQSGW+DMFT. The bandstructure and orbital characters are essentially the same as those of La<sub>0.8</sub>Ba<sub>0.2</sub>NiO<sub>2</sub>. the total spectral function shows that there are two bands crossing the Fermi level. Of these two bands, the lower energy

band shows strong two dimensional character, and it is dominated by the Ni- $d_{x^2-y^2}$  orbitals. The remaining band, the so called self-doping band, is a higher energy band which shows strong hybridization between other Ni orbitals and La orbitals. The band dispersion varies strongly along the direction normal to the Ni-O plane ( $\hat{z}$ ), demonstrating the strong 3-dimensional character of the self-doping band [11]. Moreover, the orbital character of the self-doping band is strongly dependent on  $k_z$ . In the  $k_z=0$  plane, the orbital character of the self-doping band is mostly La- $d_{z^2}$  and Ni- $d_{z^2}$  [12, 13], In contrast, in the  $k_z = \pi/c$  plane, where  $c$  is the lattice constant along the  $\hat{z}$  direction, its orbital character is mostly La- $d_{xy}$  and Ni- $p_z$ .

### FERMI-SURFACE

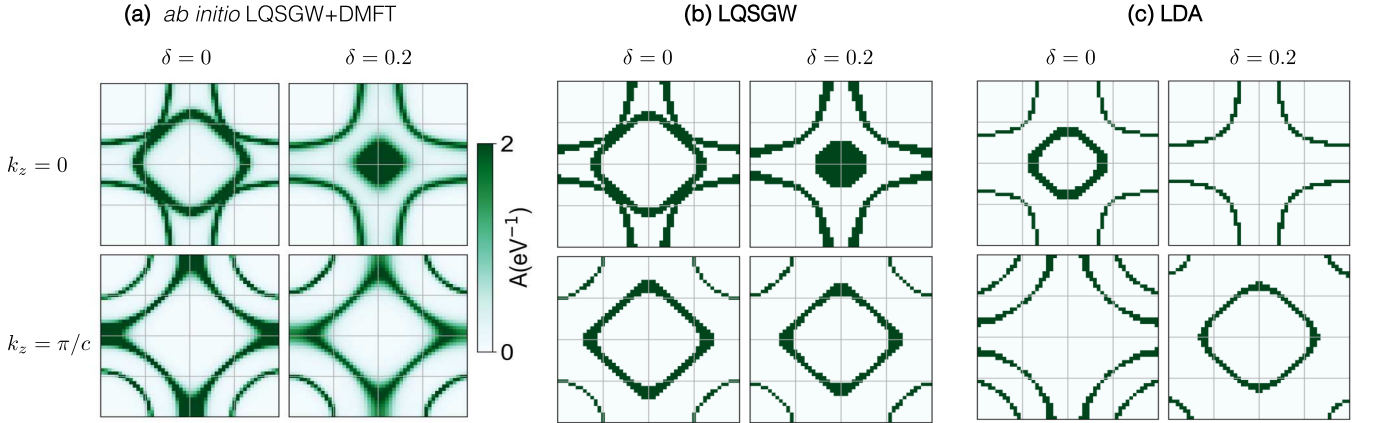


FIG. 2.  $\text{La}_{1-\delta}\text{Ba}_\delta\text{NiO}_2$  Fermi surface in the  $k_z = 0$  plane and  $k_z = \pi/c$  plane within (a) *ab initio* LQSGW+DMFT, (b) LQSGW and (c) LDA

Fig. 2 shows  $\text{La}_{1-\delta}\text{Ba}_\delta\text{NiO}_2$  Fermi surface in the  $k_z = 0$  plane and  $k_z = \pi/c$  plane and compares three different methodologies of *ab initio* LQSGW+DMFT, LQSGW and LDA. In comparison to LDA, where the electron pocket in the  $k_z = 0$  disappears at the 0.2 Ba doping, the electron pocket within *ab initio* LQSGW+DMFT and LQSGW is still present at the 0.2 Ba doping. Within *ab initio* LQSGW+DMFT, two dimensionality of Ni- $d_{x^2-y^2}$  hole-pocket is strong and it is robust against Ba-doping. As shown in Fig. 2 (a), the position and size of Ni- $d_{x^2-y^2}$  hole-pocket in  $k_z = 0$  plane are similar to those in  $k_z = \pi/c$  plane. In addition, these do not change by Ba-doping. This is in sharp contrast to LQSGW where two dimensionality of the Ni- $d_{x^2-y^2}$  hole-pocket is weaker [14] and LDA where Ni- $d_{x^2-y^2}$  hole-pocket shape is strongly affected by Ba doping.

## DOPING DEPENDENCE OF ORBITAL OCCUPATION

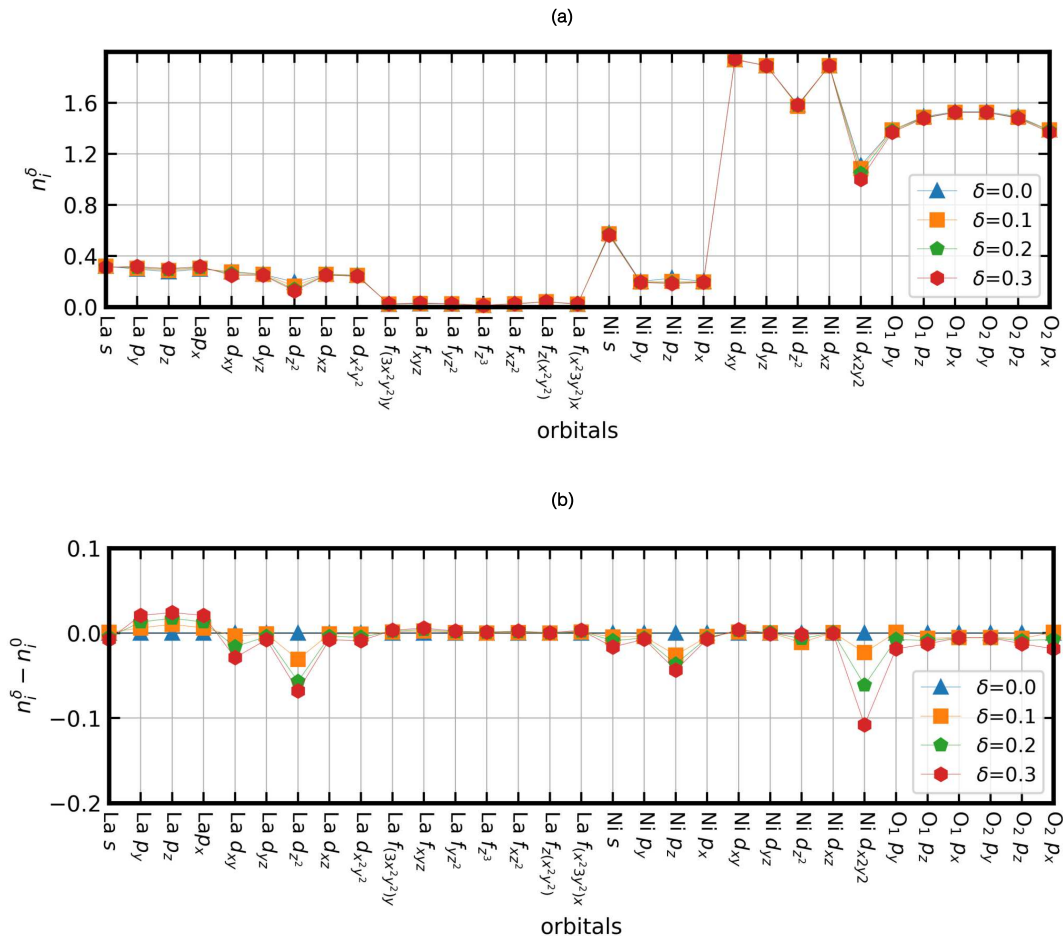


FIG. 3. (a) The doping dependence of orbital occupation. (a) Doping induced orbital occupation change

Fig. 3 shows the doping dependence of orbital occupation. In the undoped compound, Ni- $t_{2g}$  orbitals are almost fully filled. In contrast, Ni- $e_g$  orbitals are partially filled. Due to the self-doping effect, Ni- $d_{x^2-y^2}$  orbital is away from half-filling. Upon Ba doping, the occupation of Ni- $d_{x^2-y^2}$  approaches to half-filling [15, 16]. Up to 30% Ba doping, only  $\sim 30\%$  of the doped hole goes into Ni- $d$  orbitals, especially Ni- $d_{x^2-y^2}$ , but all the remaining holes go into other orbitals, especially La- $d_z$ , La- $d_{xy}$  and Ni- $p_z$ .

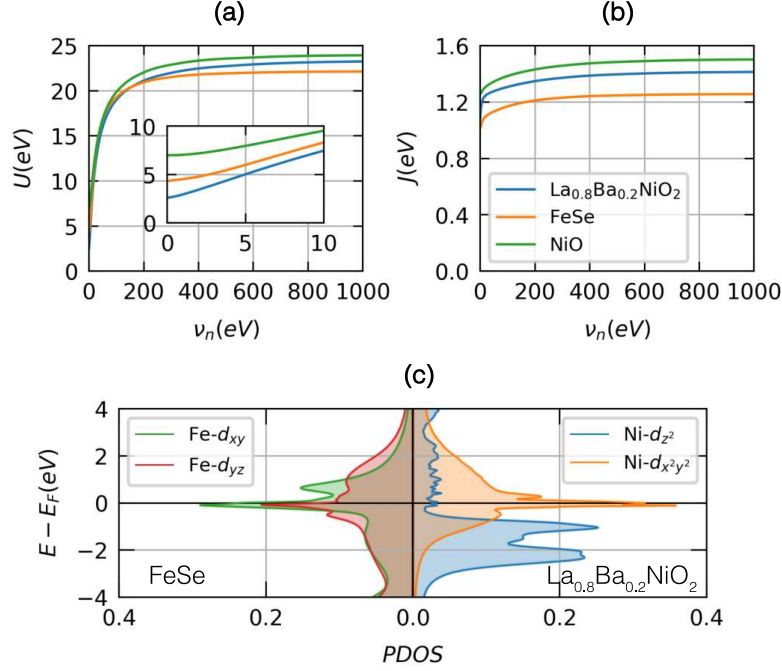
COMPARISON OF  $U$ ,  $J$ , AND PDOS BETWEEN  $\text{La}_{0.8}\text{Ba}_{0.2}\text{NiO}_2$  AND FESE

FIG. 4. (a)  $U$  and (b)  $J$  for Ni- $d$  orbitals in  $\text{La}_{0.8}\text{Ba}_{0.2}\text{NiO}_2$ , Fe- $d$  orbitals in FeSe, and Ni- $d$  orbitals in NiO within the constrained random phase approximation. In the static limit, the  $U$  of the Ni- $d$  orbitals in  $\text{La}_{0.8}\text{Ba}_{0.2}\text{NiO}_2$  is much smaller than in NiO and even smaller than that of the Fe- $d$  orbitals in FeSe. In the entire frequency range, the  $J$  for Ni- $d$  orbitals in  $\text{La}_{0.8}\text{Ba}_{0.2}\text{NiO}_2$  is larger than the  $J$  of Fe- $d$  orbitals in FeSe. Projected density of states to  $\text{La}-e_g$  orbitals in  $\text{La}_{0.8}\text{Ba}_{0.2}\text{NiO}_2$  and  $\text{Fe}-t_{2g}$  orbitals in FeSe

Based on the Coulomb interaction calculation within the constrained random phase approximation (cRPA), it is legitimate to assume the dominance of Hundness over “Mottness” in  $\text{La}_{1-\delta}\text{Ba}_\delta\text{NiO}_2$ . Fig. 4 shows the on-site Hubbard and Hund interactions among five Ni- $d$  orbitals within the constrained random phase approximation. For comparison, we plotted the  $U$  and  $J$  of Ni- $d$  orbitals in NiO and Fe- $d$  orbitals in FeSe. As is typical,  $U$  is strongly frequency dependent, while  $J$  is not. Interestingly, the static  $U$  of the Ni- $d$  orbitals in  $\text{La}_{0.8}\text{Ba}_{0.2}\text{NiO}_2$  is much smaller than it is in the charge-transfer insulator NiO. It is even smaller than the  $U$  of Fe- $d$  orbitals in the Hund’s metal FeSe. In contrast, the  $J$  of the Ni- $d$  orbitals in  $\text{La}_{0.8}\text{Ba}_{0.2}\text{NiO}_2$  is even larger than the  $J$  of Fe- $d$  in the Hund’s metal FeSe. Judging from the fact that the Ni- $e_g$  orbitals in  $\text{La}_{1-\delta}\text{Ba}_\delta\text{NiO}_2$  and the Fe- $t_{2g}$  orbitals in FeSe show similar bandwidths, we can safely assume the dominant role of Hundness over Mottness in  $\text{La}_{1-\delta}\text{Ba}_\delta\text{NiO}_2$ .

- 
- [1] A. Kutepov, V. Oudovenko, and G. Kotliar, *Computer Physics Communications* **219**, 407 (2017).
  - [2] M. A. Hayward and M. J. Rosseinsky, *Solid State Sciences International Conference on Inorganic Materials 2002*, **5**, 839 (2003).
  - [3] S. Choi, P. Semon, B. Kang, A. Kutepov, and G. Kotliar, *Computer Physics Communications* **244**, 277 (2019).
  - [4] F. Aryasetiawan, M. Imada, A. Georges, G. Kotliar, S. Biermann, and A. I. Lichtenstein, *Phys. Rev. B* **70**, 195104 (2004).
  - [5] F. Aryasetiawan, K. Karlsson, O. Jepsen, and U. Schnberger, *Phys. Rev. B* **74**, 125106 (2006).
  - [6] T. Miyake and F. Aryasetiawan, *Phys. Rev. B* **77**, 085122 (2008).
  - [7] P. Werner, M. Casula, T. Miyake, F. Aryasetiawan, A. J. Millis, and S. Biermann, *Nat Phys* **8**, 331 (2012).
  - [8] J. C. Slater, *Quantum Theory of Atomic Structure* (McGraw-Hill, 1960) google-Books-ID: W8NEAAAAIAAJ.
  - [9] S. Sugano, *Multiplets of Transition-Metal Ions in Crystals* (Elsevier, 2012).
  - [10] J. M. Tomczak, *J. Phys.: Conf. Ser.* **592**, 012055 (2015).
  - [11] M. Hepting, D. Li, C. J. Jia, H. Lu, E. Paris, Y. Tseng, X. Feng, M. Osada, E. Been, Y. Hikita, Y.-D. Chuang, Z. Hussain, K. J. Zhou, A. Nag, M. Garcia-Fernandez, M. Rossi, H. Y. Huang, D. J. Huang, Z. X. Shen, T. Schmitt, H. Y. Hwang,

- B. Moritz, J. Zaanen, T. P. Devereaux, and W. S. Lee, *Nature Materials* **19**, 381 (2020), number: 4 Publisher: Nature Publishing Group.
- [12] K.-W. Lee and W. E. Pickett, *Phys. Rev. B* **70**, 165109 (2004).
  - [13] F. Lechermann, *Phys. Rev. B* **101**, 081110 (2020), publisher: American Physical Society.
  - [14] V. Olevano, F. Bernardini, X. Blase, and A. Cano, *Phys. Rev. B* **101**, 161102 (2020), arXiv: 2001.09194.
  - [15] I. Leonov, S. L. Skornyakov, and S. Y. Savrasov, *Phys. Rev. B* **101**, 241108 (2020), publisher: American Physical Society.
  - [16] F. Petocchi, V. Christiansson, F. Nilsson, F. Aryasetiawan, and P. Werner, arXiv:2006.00394 [cond-mat] (2020), arXiv: 2006.00394.